Demonstration of Software Reconfigurable Real-Time FEC-Enabled 4/16/64-QAM-OFDM Signal Transmission in an X-Band RoF System

Ming Chen,[1,2,3*] Xin Xiao,[1] Jianjun Yu,[1,4] Fan Li,[1] Zhao Rena Huang,[2] and Hui Zhou[3]

[1]ZTE (TX) Inc., Morristown, NJ 07960, USA
[2]Department of Electrical, Computer, and System Engineering, Rensselaer Polytechnic Institute, NY 12180, USA
[3]College of Physics and Information Science, Hunan Normal University, Changsha 410081, China
[4]MOE, Fudan University, Shanghai 200433, China
*cm.ccsu@126.com

Abstract: In this work, to the best of our knowledge, this is the first time to demonstrate the generation and reception of on-line software reconfigurable real-time 4/16/64-quadrature amplitude modulation (QAM)-encoded and forward error correction (FEC)-enabled orthogonal frequency-division multiplexing (OFDM) signals over X-band fiber-over-radio (RoF)-based upstream links. A Reed-Solomon code, RS (288, 256), with symbol interleaving/de-interleaving is applied to enhance bit error rate (BER) performance. The experimental results show that, the 4/16/64-QAM-OFDM signals with net data rates of 1.6/3.2/4.8-Gb/s after 1.5-m wireless and 2.26-km SMF-28 transmission with BERs below the hard-decision FEC (HD-FEC) threshold of 3.8e-3 can be successfully achieved without using FEC. With the help of symbol-interleaved RS code, a post-FEC BER below 1e-8 can be observed when the pre-FEC BER is around 1e-3.

Index Terms: Radio over fiber (RoF), orthogonal frequency-division multiplexing (OFDM), X-band, digital signal processing (DSP), forward error correction (FEC), Reed-Solomon codes, software reconfigurable.

1. Introduction

The rapid growth in mobile data traffic caused by various mobile applications, such as mobile Internet and the Internet of Things (IoT), is making even higher-capacity transmission a more urgent goal [1-2]. The 5th generation (5G) mobile network is expected to provide a data rate up to several gigabits per second [3-4]. In recent years, radio over fiber (RoF) technology has been extensively studied [4-8] due to its numerous advantages such as broad bandwidth and low attenuation characteristics. To combat chromatic and polarization-mode dispersions in optical fiber, RoF combined with orthogonal frequency-division multiplexing (OFDM) technique which is widely used in conventional wire- and wireless communication systems, i.e., OFDM-RoF, has attracted much attention for future gigabit broadband access networks and been mainly investigated by means of off-line digital signal processing (DSP) approaches [10-12]. In addition, software-defined approach can make fiber-wireless (FiWi) networks more flexible and cost-efficient in meeting user demands when coexisting with legacy systems and devices [13]. Recently, lots of real-time demonstration works have been reported in both long-haul coherent optical OFDM (CO-OFDM) [14-16] and short-reach direct-detection OFDM (DDO-OFDM) systems [17-19]. However, as far as we know, generation and reception of software reconfigurable real-time OFDM-RoF signals for software-defined FiWi networks have not been found in this field. To make this technology practical, the hardware implementation of DSP-enabled OFDM transceivers should be performed and further investigated in RoF links.

In this paper, we experimentally demonstrate, for the first time, a real-time software reconfigurable, forward error correction (FEC) enabled and field programmable gate arrays (FPGA)-based X-band (8-12 GHz) OFDM-RoF system with a low-cost directly modulated laser (DML) for upstream link. Quadrature phase shift-keying (QPSK) or 4-ary quadrature amplitude modulation (4-QAM), 16-QAM and 64-QAM modulation formats can be dynamically configured to provide different data rate services for software-defined FiWi networks. To enhance bit error rate (BER) performance as well as improve receiver sensitivity, a Reed-Solomon code, RS (288, 256), with a coding overhead of 12.5% is also applied in the real-time OFDM-RoF system. The BER performance of uncoded and coded 4/16/64-QAM-OFDM-RoF signals is evaluated in real-time. It exhibits a significant improvement in BER performance by using RS code and a post-FEC BER of less than 1e-8 when the pre-FEC BER is about 1e-3 can be successfully achieved.

2. Experimental setup for upstream transmission of real-time OFDM-RoF singals at X-band

The experimental setup for demonstration of the real-time software reconfigurable and FEC-enabled 10-GHz OFDM-RoF signals transmission over 1.5-m wireless and 2.26-km SMF-28 for upstream link, is illustrated in Fig. 1. The key DSP algorithms in the FPGA-based baseband OFMD transceiver can be found in our previous works [20-21]. For the baseband transmitter, a pseudo-random binary sequence (PRBS) offline generated by Matlab program, which is stored in the read only memory (ROM) on the transmitter FPGA for BER test. The stored PRBS bits are encoded by 10 parallel RS (288, 256) encoders, followed by multiple-symbol interleaving [21], and then mapped to 4/16/64-QAM complex symbols. To achieve a real-valued inverse fast Fourier transform (IFFT) output, the input vector for the IFFT should have complex-conjugate

symmetry, i.e., Hermitian symmetry. After IFFT operation, the mapped QAM symbols are modulated on the data-carrying subcarriers (SCs). A certain length of cyclic prefix (CP) is appended at the beginning of IFFT outputs. Here, 100 SCs with the indexes form 1 to 100 are used to carry mapped symbols, 27 high-frequency SCs at the edge of spectrum for oversampling and direct current (DC) SC are all filled with zeros. The IFFT size and CP length are 256 and 16, respectively. To balance digital clipping noise and digital-to-analog converter (DAC) quantization noise, the digital clipping ratio (CR) is set to 12.5 dB [20]. The clipped data is scaled and fed into a DAC interface module, and then sent to a 14-bit 2.5-GS/s DAC. It should be noted that, for the sake of simplicity, the DAC and analog-to-digital converter (ADC) are clocked by a common 2.5-GHz clock source to avoid the sampling clock frequency offset effects. Fig. 2(a) shows the power spectrum of the converted signal. It exhibits that there are some images decrease in amplitude beyond Nyquist frequency (1.25-GHz), due to the zero-order-hold characteristic of the DAC. A 625-MHz clock generated by DAC/ADC is fed into the transmitter/receiver FPGA, and then divided by 4 in the DAC/ADC interface module, which output a 156.25 MHz clock for the 16-channel parallel DSP algorithm modules in the transmitter/receiver FPGA. Here, a frame OFDM consists of a random 512-point bipolar non-return-to-zero (NRZ)-encoded pattern for symbol timing synchronization, 4 training sequences (TSs) for channel estimation, and followed by 288 data-carrying OFDM symbols. So the net data rates for 4-, 16-, and 64-QAM-encoded baseband OFDM signals are, respectively, 1.6, 3.2 and 4.8-Gb/s after excluding overheads.

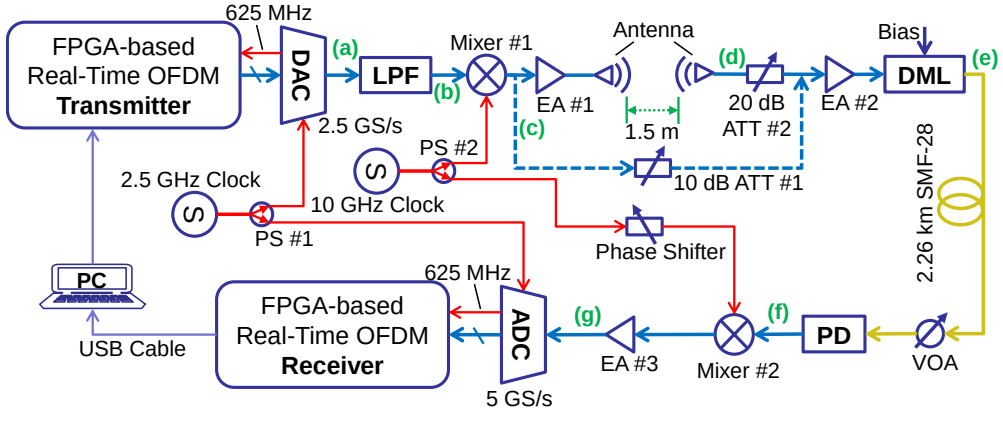

Fig. 1. Experimental setup for upstream transmission of software reconfigurable real-time OFDM-RoF signals at X-band. DAC: digital-to-analog converter, LPF: low-pass filter, PS: power splitter, EA: electrical amplifier, ATT: electrical attenuator, DML: directly-modulated laser, SMF: single-mode fiber, VOA: variable optical attenuator, PD: photo-detector, ADC: analog-to-digital converter, USB: universal serial bus, PC: personal computer.

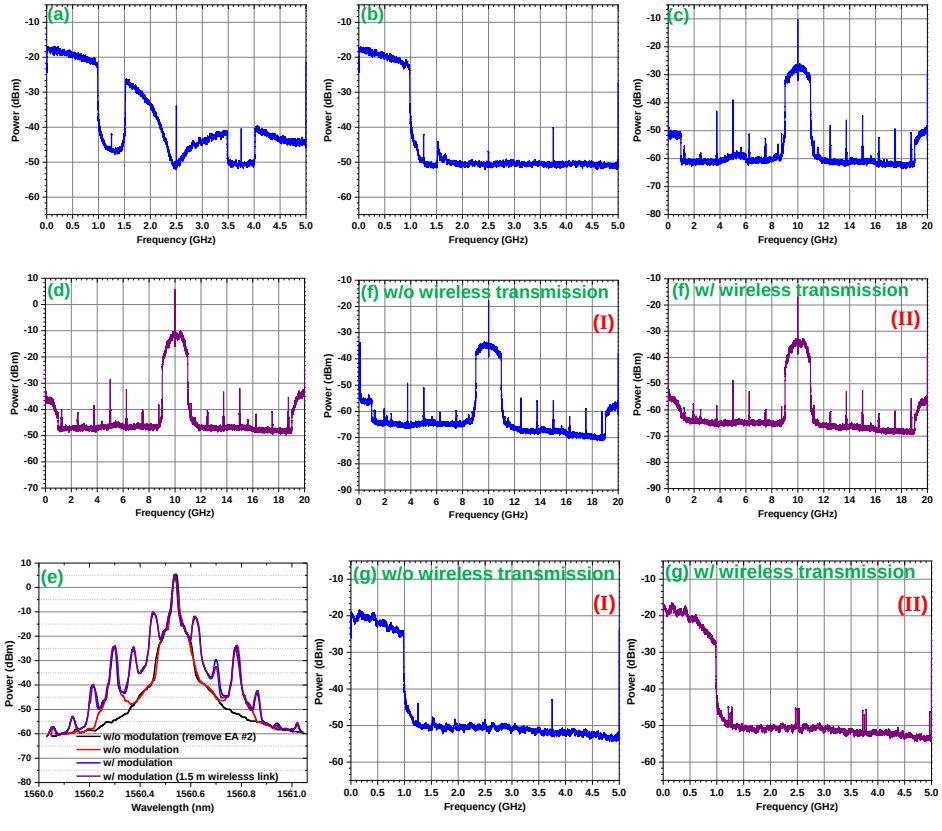

Fig. 2. Power spectra: (a) after DAC conversion, (b) after LPF filtering, (c) after mixer #1, (d) received by antenna after 1.5-m wireless transmission, (e) w/ and w/o modulation (0.02-nm resolution), (f) after PD, and (g) before ADC.

The converted baseband signal is filtered by a low-pass filter (LPF) with 3-dB bandwidth (BW) of 1-GHz, and its power spectrum is presented in Fig. 2(b). The filtered signal with a peak-to-peak voltage (Vpp) of ~ 600-mV, are then mixed with a 10-GHz sinusoidal RF source, with the power of 10-dBm after through the first power splitter (PS #1), to realize up-conversion in electrical domain. The up-converted signal with a spectrum as shown in Fig. 2(c), is boosted by an X-band electrical amplifier (EA #1) with a gain of 30-dB and a noise figure of 3, and then sent to air by a liner vertical/ horizontal polarity directional antenna. After 1.5-m wireless transmission, the RF signal can be received by another antenna. The received signal with a voltage swing of about 1.8-Vpp, having a power spectrum as given in Fig. 2(d), is first attenuated by the second 20-dB attenuator (ATT #2). The maximum wireless transmission distance (D) can be estimated approximately from the power budget (Pb) in dB as $D = D_0*10^{(Pb/20)}$, where D_0 is the initial distance with a power budget of Pb. Here D_0 = 1.5-m and Pb = 20-dB, which means that this power budget can realize at least 8×1.5 m wireless transmission when this ATT#2 is removed. For a comparison purpose, the up-converted signal is directly attenuated by a 10-dB attenuator (ATT #1) in the case of without wireless transmission. The attenuated signal is then boosted by EA #2 with 25-GHz BW and 25-dB gain. The amplified signal with a swing voltage of 3-Vpp is used to drive a 10-Gb/s DML biased at 74-mA. After electrical-to-optical (E/O) conversion, the optical double-sideband OFDM-RoF signal generated from the DML with a center wavelength of 1560.54-nm and an output power of 7.2-dBm is coupled into 2.26-km SMF-28 link without optical amplification. The optical spectra for four cases are plotted in Fig. 2(e). It should be pointed out that, EA #2 generates a sinusoidal noise at ~ 30-GHz, so we can observe that there are two wavelength components having 0.24-nm away from optical carrier in optical spectra. However, it is considered that the effect is negligible to transmission performance in our experiment. After SMF transmission, a variable optical power attenuator (VOA) is employed to change received optical power (ROP) for photo-detector (PD), followed by a PD with 15-GHz BW which is used to realize optical-to-electrical (O/E) conversion. The converted signal (see Figs. 2(f-I) and 2(f-II)) is down-converted by mixing with a phase-shifted clock from a common 10-GHz sinusoidal RF source. In the real system, the receiver side should have a clock recovery module to realize 10GHz clock recovery. It should be mentioned that, the phase shifter can be used to minimize the phase difference induced by optical fiber dispersion between local clock and the carrier of the received RF signal to attain optimal receiver sensitivity. The down-converted signal is boosted by EA #3 (45-GH BW and 20-dB gain), followed by a 10-bit 5-GS/s ADC. The spectra of the O/E converted and amplified signals are also shown in Figs. 2(g-I) and 2(g-II).

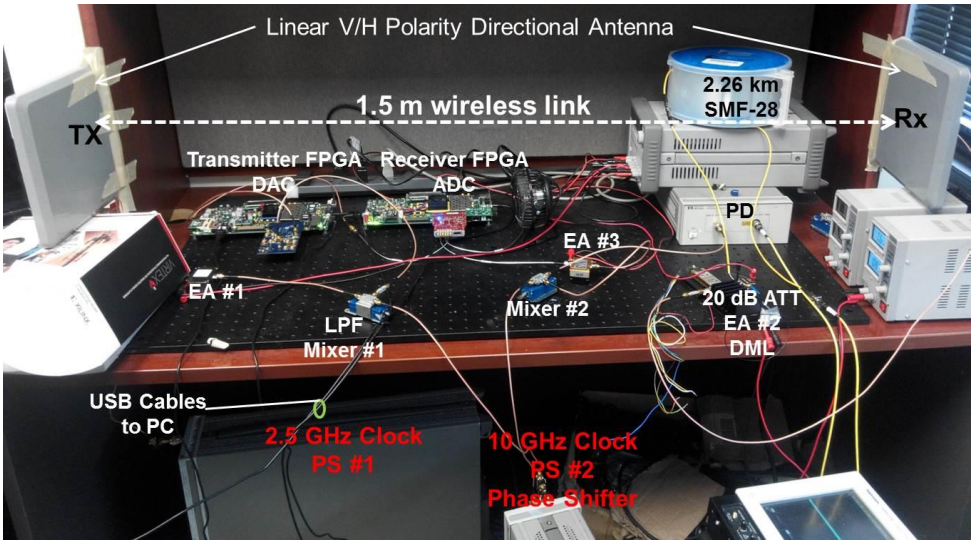

Fig. 3. Photograph of the experimental setup.

The ADC real-time captured OFDM samples are fed into the receiver FPGA via high-speed low-voltage differential signaling (LVDS) interface. The LVDS data are received through an ADC interface module in FPGA, and then sent to next function module for further processing. The DSP algorithms in the receiver FPGA include digital low-pass filtering, 2:1 down-sampling, symbol timing synchronization, CP removal, 256-point FFT operation, TS-based channel estimation and phase compensation, QAM de-mapping, and RS decoding. In addition, errors are counted over 2048 OFDM frames with a total of more than 1e8 bits. The internal FPGA signals such as real-time measured errors and only phase-compensated QAM symbols are captured and uploaded into personal computer (PC) via universal serial bus conversion (USB) cable. A photograph of the experimental setup is also given in Fig. 3.

3. Experimental results and discussion

3.1 Only 2.26-km SMF-28 link

The real-time captured only phase-compensated 64-QAM symbols on the 30th, 60th and 90th SC, without wireless transmission for optical back-to-back (OB2B) and after 2.26-km SMF-28 transmission at a ROP of 1-dBm, are shown in Fig. 4. It shows that there are increased power attenuation on these three SCs due to DAC roll-off effect and other non-perfect

frequency responses of optical and electrical devices. As we can see from Fig. 2(g-I), power on the highest SC has additional 5-dB attenuation than the SCs around DC. Here, the constellation points come from multiple non-continuous OFDM frames. After SMF transmission, the constellations with an amplitude reduction are mainly attributed to small residual phase difference between local clock and the carrier of the received RF signal caused by optical fiber dispersion. As we explained in our previous work [17], the decision threshold of QAM de-mapper for each SC depends on the corresponding estimated amplitude response, and it is equivalent to the method which has both phase and amplitude compensation with constant decision threshold values for de-mappers of all SCs. So the decreased SNRs caused by ADC quantitation noise will not lead to a significant degradation in BER performance.

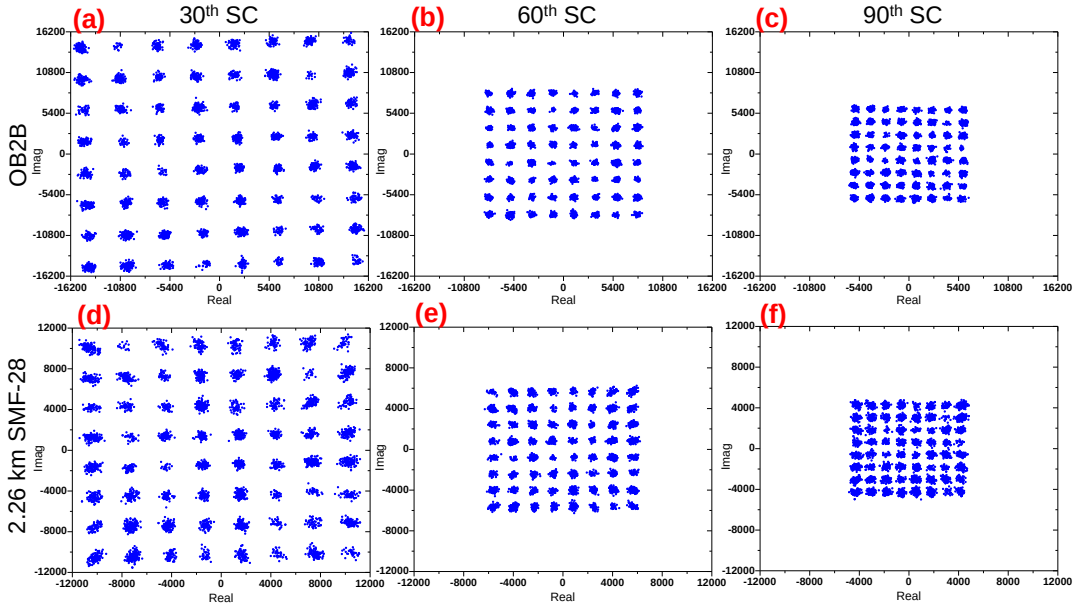

Fig. 4. Received 64-QAM constellations of different SCs without wireless transmission for (a)-(c) OB2B and (d)-(f) 2.26-km SMF-28 transmission configurations, respectively. (a), (d) 30th SC. (b), (e) 60th SC and (c), (f) 90th SC.

Fig. 5 shows the real-time measured BER performance as a function of ROP for both uncoded and coded 4/16/64-QAM-OFDM-RoF signal at OB2B and after 2.26-km SMF-28 transmission. It shows that, at a BER of 1e-3, the uncoded 4-, 16- and 64-QAM-OFDM-RoF signals transmission over 2.26-km SMF-28 link have 1, 2 and 1.5-dB power penalties, respectively. At a pre-FEC BER (or uncoded BER) of 1e-3, the post-FEC BER of 1e-8 can be achieved for all these three modulation schemes.

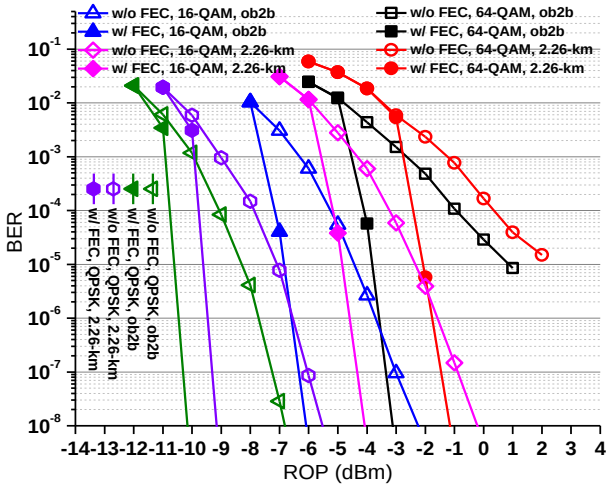

Fig. 5. Real-time BER measurements for uncoded and coded 4/16/64QAM-OFDM-RoF signal without wireless transmission.

3.2 1.5-m wireless + 2.26-km SMF-28 link

The real-time captured phase-compensated only 64-QAM symbols on the 30th, 60th and 90th SC, with 1.5-m wireless transmission for optical back-to-back (OB2B) and after 2.26-km SMF-28 transmission at a ROP of 1-dBm, are shown in Fig. 6. It shows that the 90th SC suffers higher power attenuation after wireless transmission than that of only SMF-28 transmission. This fact is due to the limited BW of X-band amplifier, EA #1, and antennas, and we can see this point clearly from Fig. 2(g-II). Bit loading (or adaptive modulation) can be used to cope with problem. It also exhibits that the 64-QAM

constellation points after wireless transmission, to some extent, are distorted.

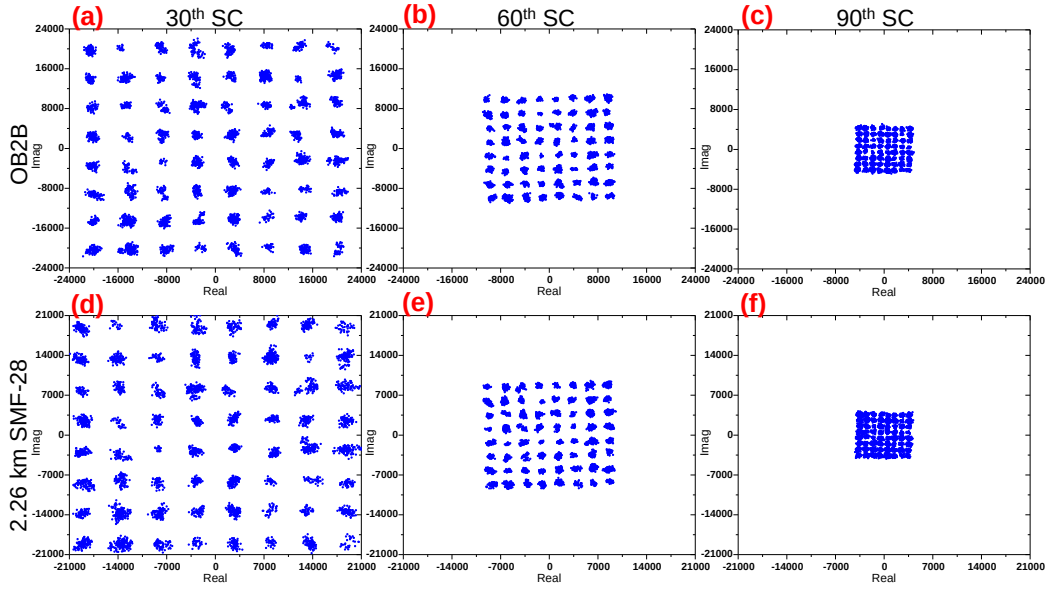

Fig. 6. Received 64-QAM constellations of different SCs after 1.5-m wireless transmission for (a)-(c) OB2B and (d)-(f) 2.26-km SMF-28 transmission configurations, respectively. (a), (d) 30th SC. (b), (e) 60th SC and (c), (f) 90th SC.

The real-time measured BER performance as a function of ROP for both uncoded and coded 4/16/64-QAM-OFDM-RoF signal at OB2B and after 2.26-km SMF-28 transmission under 1.5-m wireless transmission is presented in Fig. 7. Compared to only 2.26-km SMF-28 transmission, additional 1.5-m wireless transmission leads to additional about 1.5, 1 and 3-dB power penalty for uncoded 4, 16 and 64-QAM-OFDM-RoF signal at a BER of 1e-3, respectively. Meanwhile, at a pre-FEC BER (or uncoded BER) of 1e-3, the post-FEC BER of 1e-8 still can be achieved for all these three modulation schemes.

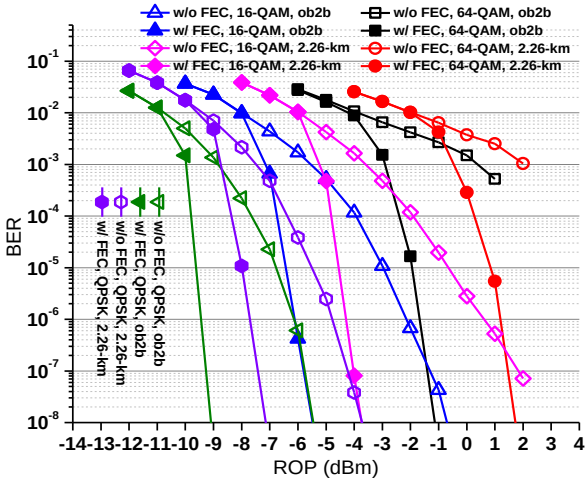

Fig. 7. Real-time BER measurements for uncoded and coded 4/16/64QAM-OFDM-RoF signal with 1.5-m wireless transmission.

4. Conclusions

We have experimentally demonstrated real-time software reconfigurable and RS (288, 256) coding-enabled 1.6/3.2/4.8-Gb/s 4/16/64-QAM-OFDM-RoF systems with a DML at X-band for upstream link, for the first time. After 1.5-m wireless and 2.26-km SMF-28 transmission, the BER below than HD-FEC threshold of 3.8e-3 can be observed without using FEC technique. Meanwhile, a post-FEC BER below 1e-8 is successfully achieved when the pre-FEC BER is 1e-3 for all these three QAM modulation schemes. In addition, the BER performance can be further enhanced if adaptive modulation is adopted in the real-time system.

Acknowledgements

This work was supported in part by the National High-Tech Research and Development Program (863 Program) of China under Grant 2015AA016904 and U.S. National Science Foundation under Grant 1128540, in part by the National Natural Science Foundation of China under Grant 61325002 and Grant 61250018, and in part by the National High-Tech Research and Development Program (863 Program) of China under Grant 2015AA016904.

References

[1] A. Gupta and R. K. Jha, “A Survey of 5G Network: Architecture and Emerging Technologies,” *IEEE Access*, vol.3, pp.1206-1232, 2015.

[2] T. Asai, “5G radio access network and its requirements on mobile optical network,” *Proc. ONDM 2015*, pp.7-11.

[3] J. Zhang, M. Xu, J. Wang, F. Lu, L. Cheng, M. Zhu; I. Khalil, J. Yu, and G.-K. Chang, “Carrier aggregation for MMW inter-RAT and intra-RAT in next generation heterogeneous mobile data network based on optical domain band mapping,” *Proc. ECOC 2015*, paper We.4.4.5

[4] M. Peng, Y. Li, Z. Zhao, and C. Wang, “System architecture and key technologies for 5G heterogeneous cloud radio access networks,” *IEEE Network*, vol.29, no.2, pp.6-14, 2015.

[5] J. Yu, Z. Jia, T. Wang, and G.-K. Chang, “A Novel Radio-Over-Fiber Configuration Using Optical Phase Modulator to Generate an Optical mm-Wave and Centralized Lightwave for Uplink Connection,” *IEEE Photon. Technol. Lett.*, vol.19, no.3, pp.140-142, 2007.

[6] L. Chen, Y. Shao, X. Lei, H. Wen, and S. Wen, “A Novel Radio-Over-Fiber System With Wavelength Reuse for Upstream Data Connection,” *IEEE Photon. Technol. Lett.*, vol.19, no.6, pp.387-389, 2007.

[7] J. Yu, G-K Chang; Z. Jia, A. Chowdhury, M.-F. Huang, H.-C. Chien, Y.-T. Hsueh, W. Jian, C. Liu, Z. Dong, “Cost-Effective Optical Millimeter Technologies and Field Demonstrations for Very High Throughput Wireless-Over-Fiber Access Systems”, *J. Lightw. Technol.*, vol. 28, no. 16, pp. 2376-2397, 2010.

[8] D. Wake, A. Nkansah, and N. J. Gomes, “Radio Over Fiber Link Design for Next Generation Wireless Systems,” *J. Lightw. Technol.*, vol.28, no.16, pp.2456-2464, 2010.

[9] M. Zhu, L. Zhang, J. Wang, L. Cheng, C. Liu, and G.-K. Chang, “Radio-Over-Fiber Access Architecture for Integrated Broadband Wireless Services,” *J. Lightw. Technol.*, vol.31, no.23, pp.3614-3620, 2013.

[10] Z. Cao, J. Yu, M. Xia, Q. Tang, Y. Gao, W. Wang, and L. Chen, “Reduction of Intersubcarrier Interference and Frequency-Selective Fading in OFDM-ROF Systems,” *J. Lightw. Technol.*, vol.28, no.16, pp.2423-2429, 2010.

[11] C.-C. Wei, C.-T. Lin, H.-T. Huang, W.-L. Liang, and S. Chi, “Estimation and Suppression of Dispersion-Induced Phase Noise in W-band Direct-Detection OFDM Radio-Over-Fiber Systems,” *J. Lightw. Technol.*, vol.32, no.20, pp.3874-3884, 2014.

[12] H. Huang, W. Liang, C. Lin, C. Wei, and S. Chi, “100-GHz DD-OFDM-RoF system over 150-km fiber transmission employing pilot-aided phase noise suppression and bit-loading algorithm,” *Opt. Express*, vol. 22, no. 4, pp. 3938-3943, 2014.

[13] A. Amate, M. Milosavljevic, P. Kourtessis, M. Robinson, and J. M. Senior; “SDN based millimetre wave radio over fiber (RoF) network,” *Proc. SPIE 9387, Broadband Access Communication Technologies IX*, p. 938706.

[14] Q. Yang, S. Chen, Y. Ma, and W. Shieh, “Real-time reception of multi-gigabit coherent optical OFDM signals,” *Opt. Express*, vol. 17, no. 10, pp. 7985-7992, 2009.

[15] N. Kaneda, T. Pfau, H. Zhang, J. Lee, Y.-K. Chen, C.-J. Youn, Y.-H. Kwon, E. S. Num, and S. Chandrasekhar, “Field demonstration of 100-Gb/s real-time coherent optical OFDM detection,” *Proc. ECOC 2014*, paper Th.2.5.3.

[16] X. Xiao, F. Li, J. Yu, X. Li, Y. Xia, and Y. Chen, “100-Gb/s Single-band Real-time Coherent Optical DP-16QAM-OFDM Transmission and Reception," *Proc. OFC 2014, Postdeadline Papers*, paper Th5C.6.

[17] X. Duan, R.P. Giddings, M. Bolea, Y. Ling, B. Cao, S. Mansoor, and J.M. Tang, "Real-time experimental demonstrations of software reconfigurable optical OFDM transceivers utilizing DSP-based digital orthogonal filters for SDN PONs," Opt. Express, vol. 22, no. 16, pp. 19674-19685, 2014.

[18] M. Chen, J. He, and L. Chen, “Real-Time Optical OFDM Long-Reach PON System Over 100-km SSMF Using a Directly Modulated DFB Laser,” *IEEE/OSA J. Opt. Commun. Netw.*, vol. 6, no. 1, pp. 18-25, 2014.

[19] X. Xiao, F. Li, J. Yu, Y. Xia, and Y. Chen, “Real-time demonstration of 100Gbps class dual-carrier DDO-16QAM-DMT transmission with directly modulated laser,” *Proc. OFC 2014*, San Francisco, CA, paper M2E.6

[20] M. Chen, J. He, Q. Fan, Z. Dong, and L. Chen, “Experimental Demonstration of Real-Time High-Level QAM-Encoded Direct-Detection Optical OFDM Systems,” *J. Lightw. Technol.*, vol. 33, no. 22, pp. 4632-4639, 2015.

[21] M. Chen, X. Xiao, X. Li, J. Yu, Z. R. Huang, F. Li, and L. Chen, “Improved BER Performance of Real-Time DDO-OFDM Systems Using Interleaved Reed-Solomon Codes,” *IEEE Photon. Technol. Lett.*, DOI: 10.1109/LPT.2016.2523268, 2016.